Indazole–Pyridine Hybrids: Design, Synthesis, and Biological Evaluation as Possible Anticancer Agents against Breast Cancer Cell Lines

Kinjal Parmar

kinjal.parmar19149@paruluniversity.ac.in

Parul University

Ishan Panchal

Parul College of Pharmacy and Research, Parul University

Research Article

Keywords: Indazole–pyridine derivatives, Molecular docking, MCF-7 cells, cytotoxic activity, ADME analysis

Posted Date: August 27th, 2025

DOI: https://doi.org/10.21203/rs.3.rs-7458469/v1

Additional Declarations: No competing interests reported.

Indazole–Pyridine Hybrids: Design, Synthesis, and Biological Evaluation as Possible Anticancer Agents against Breast Cancer Cell Lines

Kinjal Parmar1*, Ishan Panchal2
*1 Research Scholar, Department of Pharmaceutical Chemistry, Faculty of Pharmacy, Parul University, P.O.: Limda, Ta: Waghodia-391760, Vadodara, Gujarat, India
2 Department of Pharmaceutical Chemistry, Parul College of Pharmacy and Research, Faculty of Pharmacy, Parul University, P.O.: Bopal, Ahmedabad-380058, Gujarat, India

Email id of corresponding Author: kinjal.parmar0110@gmail.com

Orcid id: https://orcid.org/0000-0002-0551-0363

ABSTRACT

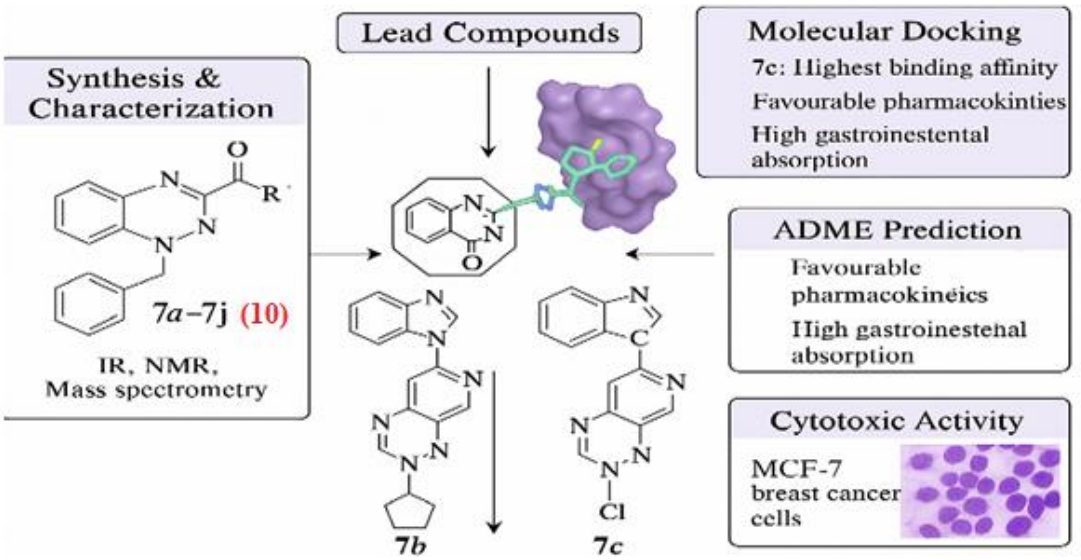

A novel series of (3-amino-5-methyl-1H-indazol-1-yl)(5-substituted-pyridin-3-yl)methanone derivatives (7a–7j) was synthesized and structurally confirmed using IR, NMR, and mass spectrometry. Molecular docking analysis performed with AutoDock identified compound 7c as the most potent binder (–8.7 kcal/mol), surpassing the standard drug Entrectinib. Compounds 7i and 7e also demonstrated favorable interactions, suggesting their potential as lead molecules. Predicted ADME features include high gastrointestinal absorption and minimal inhibition of cytochrome P450 enzymes, leading to good oral availability. In vitro cytotoxicity tests on MCF-7 breast cancer cells demonstrated that compounds 7b and 7c produced strong antiproliferative effects, with 7c achieving up to 64% reduction in cell viability, approaching the efficacy of Adriamycin. Moderate activity was observed in compounds 7d, 7g, and 7i, whereas 7a, 7e, and 7f displayed weak activity. Overall, compounds 7b and 7c emerge as promising candidates for further optimization, with structural elements such as cyclopentyl and halogen substituents contributing significantly to their biological activity. These results provide a foundation for mechanistic exploration and development of new anticancer agents.

Keywords: Indazole–pyridine derivatives, Molecular docking, MCF-7 cells, cytotoxic activity, ADME analysis

INTRODUCTION:

Cancer is a disease that causes uncontrolled cell proliferation, disrupting normal tissue processes. Malignant progression can cause serious physiological consequences and constitute a significant risk. A threat to human life. Despite advancements in prevention and treatment, cancer remains a major worldwide health concern. Since 1991,

over four million cancer-related deaths have been avoided due to reduced tobacco use, early identification, and better treatment choices. [1].

Breast cancer is one of the most common malignancies among women, accounting for the second highest cause of cancer-related deaths overall and the first among Black and Hispanic women. Between 1989 and 2022, the breast cancer mortality rate decreased by 44%, resulting in 517,900 fewer fatalities [2]. However, the disease remains a big concern in nations such as India, where female breast cancer is the most prevalent, accounting for 13.5% of new cases and 10% of cancer-related deaths in 2020 [3]. With India ranked third internationally after China and the United States, GLOBOCAN projects that cancer incidence would climb to 2.08 million cases by 2040, representing a 57.5% increase from 2020 [4]. These troubling developments highlight the critical need for new, effective, and accessible treatment techniques.

Recent advancements in molecular oncology have enabled the creation of tailored medicines that increase survival while reducing systemic toxicity [5-12]. Among potential targets, tropomyosin receptor kinases (Trk), encoded by the NTRK1, NTRK2, and NTRK3 genes, have gained attention due to their critical role in neural development and involvement in oncogenic processes. Abnormalities in Trk signaling—such as gene fusions, overexpression, and activating mutations—have been implicated in breast cancer initiation, progression, and metastasis [13].

NTRK Gene Fusions

Chromosomal rearrangements involving NTRK genes lead to constitutively active Trk fusion proteins that drive oncogenic signaling. Although rare in breast cancer (<1% of cases), NTRK fusions are frequently identified in secretory breast carcinoma (SBC), where ETV6–NTRK3 fusions are a hallmark. Reports also suggest the occurrence of NTRK1 fusions in non-secretory subtypes, highlighting their broader, albeit uncommon, role in breast cancer biology [14].

TrkA (NTRK1) Overexpression

Overexpression of TrkA has been documented in more than 20% of breast cancers, including triple-negative breast cancer (TNBC). Experimental models demonstrate that TrkA overexpression promotes growth factor–independent proliferation and enhances migratory capacity through activation of PI3K and MAPK pathways. Importantly, these effects can be suppressed by Trk inhibitors such as larotrectinib, supporting the therapeutic potential of targeting Trk signaling [14].

Trk inhibitors, such as larotrectinib and entrectinib, have already shown clinical success in tumors with NTRK fusions, resulting in FDA approval for the treatment of NTRK fusion-positive solid tumors. Current studies are expanding this treatment approach to breast tumors with Trk overexpression, potentially broadening the clinical applicability of these inhibitors [15]. Figure 1 illustrates the chemical structures of FDA-approved anticancer medicines.

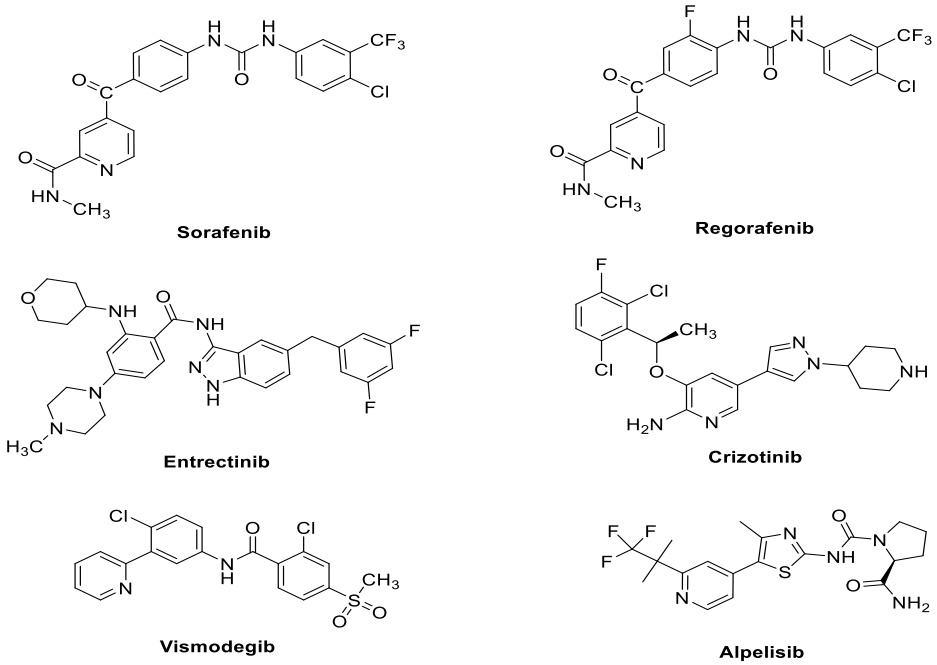

Fig 1. Chemical structures of FDA-approved anticancer drugs

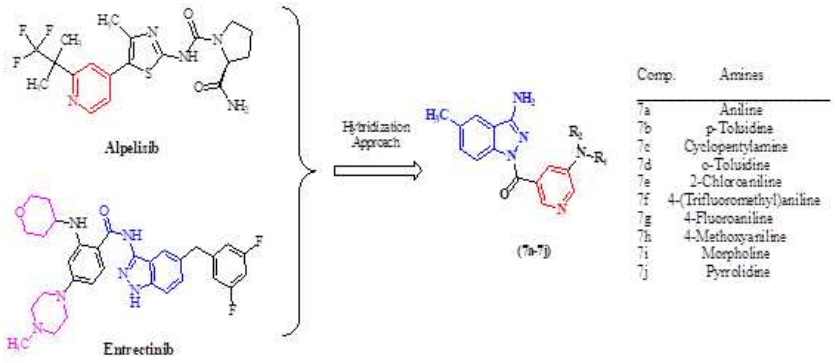

Fig 2. Design strategy for indazole-pyridine hybrids (Target compounds 7a-7j)

EXPERIMENTAL WORK

Materials

Analytical chemicals and reagents were sourced from reputable sources like Sigma-Aldrich, Merck, and Alfa Aesar. Solvents were purified and dried following conventional laboratory methods. Indazole and other beginning ingredients were applied immediately without additional purification is required, unless otherwise noted. Column chromatography was done with silica gel (60-120 mesh). Thin-layer chromatography on silica gel plates (Merck) was used to monitor reaction progress. UV light was used at 254 and 366 nm for visualization. Melting points were measured using an open capillary technique and given without correction. Figure 3 shows the synthesis pathway for indazole-based derivatives.

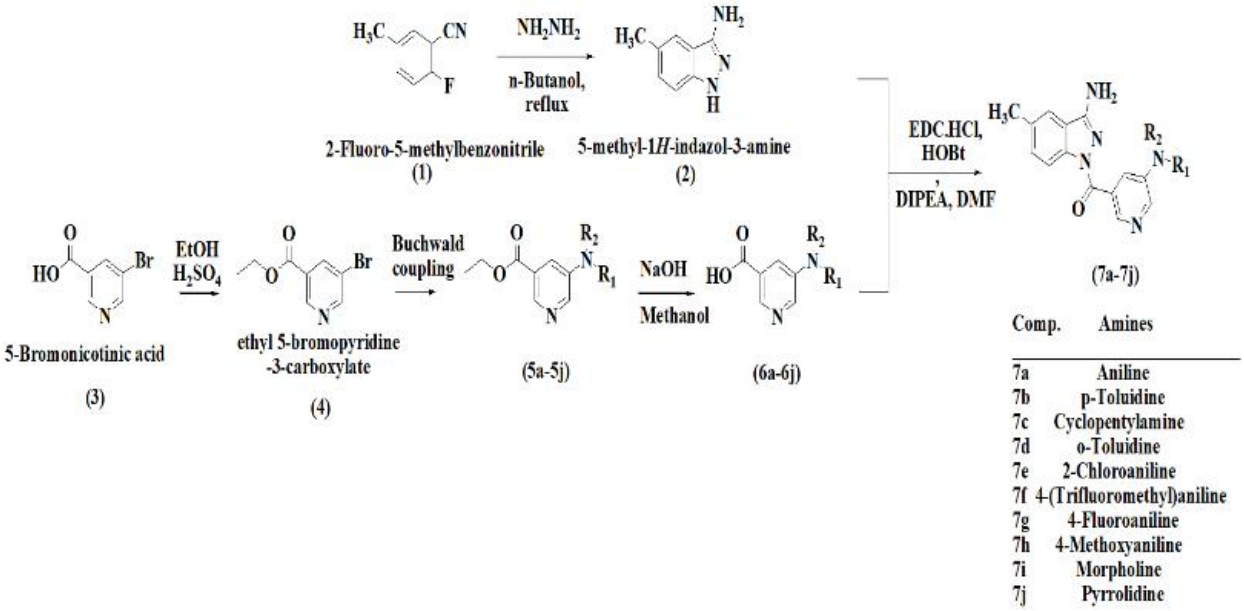

Fig 3. Scheme for the synthesis of indazole-based derivatives

Instrumentation

IR spectra were collected using a Bruker FTIR spectrophotometer with KBr pellets. ^{1}H-NMR and ^{13}C-NMR spectra were recorded on Bruker instruments (400 or 500 MHz) using DMSO-d_6 or $CDCl_3$, with TMS as an internal standard. The Waters LC-MS/MS system was employed for mass spectrometry with an electrospray ionization (ESI) source.

Synthesis of 5-methyl-1H-indazol-3-amine (2) from 2-fluoro-5-methyl benzonitrile (1):

5-Bromo-3-nicotinic acid (5.0 g, 24.75 mmol) was dissolved in 50 mL ethanol at room temperature. The liquid was refluxed for 10 hours after adding 5.3 mL of concentrated sulfuric acid (99.0 mmol) dropwise and stirring continuously. Reaction progress was monitored by TLC. After completion, the solution was cooled to 0°C and neutralized with saturated sodium carbonate (pH ≈ 8). The product was obtained by extracting the mixture with chloroform (3 x 50 mL), drying it with Na_2SO_4, and concentrating it under reduced pressure.

Note: Spectral interpretation data, such as IR, Mass, and NMR of 5-methyl-1H-indazol-3-amine are Provided in the supplementary materials.

Synthesis of Ethyl 5-bromopyridine-3-carboxylate (4) from 5-Bromonicotinic acid (3)

Ethyl alcohol (50 mL) was used to dissolve 5-bromo-3-nicotinic acid (5.00 g, 24.75 mmol) at room temperature. Concentrated sulfuric acid (5.3 mL, 99.0 mmol) was added to this solution drop by drop while being continuously stirred. Once the addition was finished, the reaction mixture was refluxed for ten hours. TLC kept an eye on the reaction's development. Following reaction completion, the reaction mixture was neutralized with a saturated sodium carbonate solution (pH=8) and chilled to 0 °C. After neutralizing the solution, it was dried using Na2SO4 and extracted using 3 x 5 ml of chloroform. Ethyl 5-bromo-3-nicotinate was obtained by evaporating the gathered organic layer at a lower pressure.

Common methodology for synthesis of intermediates (5a–5j)

In a 50 mL round-bottom flask, 5 ml of anhydrous DMF was used to dissolve 0.1 mol of ethyl 5-bromopyridine-3-carboxylate, which was then agitated for 15 minutes at 40 °C. The matching substituted amine was added after sodium tertibutoxide (0.1 mol) and $Pd_2(dba)_3$ (0.1 mol) were added. At 90 °C, the mixture was agitated until the reaction was complete, as shown by TLC. The concoction was poured into 250 milliliters of ice-cold water, and the solid that formed was filtered and then recrystallized from ethanol.

Note: Spectral interpretation data, such as IR, Mass, and NMR of compound 5a to 5j are provided in the supplementary materials.

Common methodology for synthesis of acids (6a–6j)

The intermediates (5a-5j, 1.0 g, 4.13 mmol) were dissolved in methanol (50 mL). Aqueous NaOH solution (0.83 g in 5 mL, 20.65 mmol) was added, and the mixture was refluxed at 65 degrees Celsius for 14-16 hours. The reaction mixture was concentrated under reduced pressure, and the residue was dissolved in a small amount of water (3-5 ml). Acidification with glacial acetic acid (pH ≈ 3) precipitated the product, which was then filtered and vacuum-dried.

Note: Spectral interpretation data, such as IR, Mass, and NMR of compound 6a to 6j are provided in the supplementary materials.

Common methodology for synthesis of final compounds (7a-7j)

A solution of acids (6a-6j) in DMF (10 mL) was treated with DIPEA (1.18 mL, 6.80 mmol), cooled to 0 °C, and then added EDC-HCl (1.30 g, 6.80 mmol), 5-methyl-1H-indazol-3-amine (2) (0.5 g, 3.40 mmol), and HOBt (0.92 g, 6.80 mmol). The mixture was stirred at room temperature for five hours. After completion (monitored by TLC), the mixture was put into ice-cold water (25 mL) and extracted with ethyl acetate (3 x 25 mL). The organic layer was dried on Na_2SO_4, filtered, and concentrated. The crude residue was refined using silica gel column chromatography (chloroform/methanol) to yield compounds 7a-7j.

Note: Spectral interpretation data, such as IR, Mass, and NMR of compound 7a to 7j are provided in the supplementary materials.

Molecular Docking studies:

Docking studies were carried out in Auto Dock Vina. Table 4 summarizes the docking study results. The results show strong affinity between the proposed compounds and the target enzyme, indicating their potential for further development.

Retrieval and Preparation of Target Protein (PDB ID: 5JFX)

The Protein Data Bank (https://www.rcsb.org/) provided a three-dimensional structure of human CDK7 in complex with Cyclin H and MAT1 (PDB ID: 5JFX). PyMOL and AutoDock Tools (ADT) were used to process the protein, removing any unnecessary components. The water molecules, ions, and co-crystallized ligands were all eliminated. Hydrogen atoms were added to enhance bonding, and Kollman charges were assigned. The generated structure was saved in PDBQT format for docking experiments.

Ligand Preparation

The chemical structures of the synthesized derivatives (7a–7j) were sketched using ChemDraw Ultra 12.0, and energy minimization was carried out in Chem3D 12.0. The optimized ligands were converted into PDB format and subsequently transformed into PDBQT format using AutoDock Tools 1.5.6.

Docking Procedure

Docking experiments were carried out using AutoDock Vina. The docking grid box was set at 60 Å × 60 Å × 60 Å with an exhaustiveness parameter of 8, ensuring adequate space for ligand movement within the active site. We docked each ligand (7a-7j) against TrkA and assessed conformations based on binding energy values (kcal/mol). Binding poses were displayed and investigated using Discovery Studio Visualizer 19.0. (https://discover.3ds.com/)

Validation of docking protocol

The co-crystallized ligand from PDB ID: 5JFX was redocked into the active site to confirm the docked technique. Determined was the root-mean-square deviation (RMSD) between the docked position and the crystallographic position. A value less than 2.0 Å was considered acceptable to showcase the reproducibility of the docked protocol.

Docking Results

The produced compounds showed binding affinities between -6.3 and -8.7 kcal/mol. The chemical with the highest binding affinity (–8.7 kcal/mol) among them was compound 7c, which outperformed the common medication Entrectinib (–8.4 kcal/mol). While compounds 7a, 7g, 7h, and 7j displayed relatively lesser binding (–6.3 to –6.8 kcal/mol), compounds 7i (-8.5 kcal/mol) and 7e (–8.2 kcal/mol) also had substantial interactions. These findings point to compounds 7c, 7i, and 7e as possible lead candidates for additional optimization and emphasize the importance that structural changes play in modifying binding efficiency.

In silico ADME Pharmacokinetic Studies:

The pharmacokinetic behavior of the synthesized indazole-based derivatives (7a–7j) was evaluated using the SWISSADME online platform (https://www.swissadme.ch/) provided by the Swiss Institute of Bioinformatics. Each compound was entered into the system using its SMILES notation to generate predictive profiles for absorption, distribution, metabolism, and excretion (ADME).

Physicochemical Parameters

Key physicochemical descriptors such as lipophilicity (calculated by multiple algorithms, including iLOGP) and aqueous solubility (LogS) were analyzed. These properties provided insights into drug-likeness and oral bioavailability.

Absorption and Distribution

All compounds were predicted to have high gastrointestinal (GI) absorption, indicating favorable potential for oral delivery. Blood–brain barrier (BBB) penetration was observed only for compound 7j, suggesting possible central nervous system activity. The remaining derivatives were predicted to be restricted to peripheral tissues.

Metabolism

Cytochrome P450 (CYP) enzyme inhibition was also assessed. Most compounds were predicted to inhibit CYP1A2, CYP2C9, and CYP2D6, indicating the possibility of drug–drug interactions. Inhibition of CYP2C19 was limited to compounds 7a and 7e. Notably, compound 7j showed minimal CYP inhibition, reflecting a lower risk of metabolic interactions.

Excretion and Efflux

Prediction of P-glycoprotein (P-gp) substrate status suggested that compounds 7c, 7i, and 7j may undergo efflux transport, potentially affecting their oral bioavailability.

Drug-Likeness Assessment

All compounds were evaluated against established drug-likeness rules, including Lipinski's Rule of Five and Veber's criteria. Most derivatives complied with these guidelines, supporting their potential as orally active drug candidates.

Overall, the ADME analysis indicated that the designed indazole–pyridine derivatives possess favorable pharmacokinetic attributes, with compound 7j standing out due to its BBB permeability and low CYP inhibition, making it an interesting candidate for further CNS-targeted drug design.

Cell Line studies:

The Sulforhodamine B (SRB) assay, a trustworthy method for measuring cell density by total cellular protein content, was used to assess the test substances' lethal potential. Cell lines were cultivated in an appropriate growth medium that was enhanced with 2 mM L-glutamine and 10% fetal bovine serum. In 96-well microtiter plates with 100 µL of media per well, about 5,000 cells were seeded. The plates were then incubated for 24 hours at 37 °C in a humidified environment with 5% CO_2 and 95% air. The test substances were added at different quantities after this initial incubation, and the cells were then incubated once more to assess their reaction. After treatment, cellular proteins were stained with SRB dye, and absorbance was measured to estimate cell proliferation. The extent of cell growth was determined by comparing absorbance values of treated wells with those of untreated controls. Growth inhibition was expressed as a percentage using the equation: $\%Inhibition=(CTi)\times100$

where Ti represents the absorbance of treated cells and C corresponds to that of the control. This calculation provided an estimate of the antiproliferative activity of the tested compounds [16].

RESULT AND DISCUSSION

The synthesized compounds were evaluated based on their practical yield, melting point, solubility, and spectral characteristics. The physicochemical parameters are summarized in **Table 1**. Additionally, various other studies were conducted; **Table 2** presents the molecular property data; **Table 3** outlines the pharmacokinetic profiles;

Table 4 highlights the binding affinities of the designed molecules; and **Table 5** details the results of cell line studies. Binding interaction of some selected novel derivatives are mentioned in the figure 4.

Table 1: Physical characteristics of synthesized compounds (7a-7j)

Comp. code	Mol. Formula	%Yield	Melting point (^{o}C)	Rf value (ethyl acetate: Hexane)
7a	$C_{20}H_{17}N_5O$	67%	198-200 ^{0}C	0.32
7b	$C_{21}H_{19}N_5O$	71%	188-190 ^{0}C	0.33
7c	$C_{19}H_{21}N_5O$	68%	174-178 ^{0}C	0.32
7d	$C_{21}H_{19}N_5O$	73%	178-180 ^{0}C	0.32
7e	$C_{20}H_{16}ClN_5O$	71%	192-194 ^{0}C	0.45
7f	$C_{21}H_{16}F_3N_5O$	71%	230-232 ^{0}C	0.26
7g	$C_{20}H_{16}FN_5O$	74%	216-218 ^{0}C	0.23
7h	$C_{21}H_{19}N_5O_2$	72%	194-196 ^{0}C	0.23
7i	$C_{18}H_{19}N_5O_2$	67%	188-190 ^{0}C	0.26
7j	$C_{18}H_{19}N_5O$	65%	218-220 ^{0}C	0.34

Table 2: Molecular properties of synthesized compounds (7a-7j)

Comp. code	Molecular weight (g/mol)	H-bond acceptor (nON)	H-Bond donor (nOHNH)	iLogP	Lipinski Rule
Standard value	<500	<10	<5	<5	Yes/No
7a	343.38	3	2	2.59	Yes
7b	357.41	3	2	2.86	Yes
7c	335.40	3	2	2.97	Yes
7d	357.41	3	2	2.95	Yes
7e	377.83	3	2	3.01	Yes
7f	411.38	6	2	2.88	Yes
7g	361.37	4	2	2.71	Yes
7h	373.41	4	2	2.98	Yes
7i	337.38	4	1	2.51	Yes
7j	323.38	3	1	2.70	Yes

Table 3: Pharmacokinetic properties of synthesized compounds (7a-7j)

Comp. code	GI absorption	BBB permeation	Pgp substrate	CYP1A2	CYP2C19	CYP2C9	CYP2D6
7a	High	No	No	Yes	Yes	Yes	Yes
7b	High	No	No	Yes	No	Yes	Yes
7c	High	No	Yes	Yes	No	Yes	Yes
7d	High	No	No	Yes	No	Yes	Yes
7e	High	No	No	Yes	Yes	Yes	Yes
7f	High	No	No	Yes	Yes	Yes	Yes
7g	High	No	No	Yes	Yes	Yes	Yes
7h	High	No	No	Yes	No	Yes	Yes
7i	High	No	Yes	No	No	Yes	No
7j	High	Yes	Yes	Yes	No	Yes	No

Table 4: Binding affinity of 7a-7j

Compounds	Binding affinity (kcal/mol)
7a	-6.3
7b	-7.5
7c	-8.7
7d	-7.3
7e	-8.2
7f	-7.8
7g	-6.8

7h	-6.8
7i	-8.5
7j	-6.5
Entrectinib	**-8.4**

Table 5: Cell Line study: Human Breast Cancer Cell Line MCF-7

Human Breast Cancer Cell Line MCF-7				
% Control Growth				
Compounds	**Drug Concentrations (µg/ml) Average Values**			
	10	**20**	**40**	**80**
7a	93.62	98.18	95.02	90.20
7b	31.05	-8.63	-23.22	6.38
7c	45.78	17.73	-28.22	-64.06
7d	67.70	71.69	60.46	43.52
7e	50.22	53.66	58.72	65.24
7f	87.43	94.91	83.49	71.76
7g	39.39	40.57	40.88	46.46
7h	51.59	61.63	39.13	12.26
7i	67.53	59.31	45.49	16.48
7j	68.02	77.56	57.63	39.11
Doxurubicin	-68.6	-73.1	-78.7	-78.2
ADR	-72.69	-72.36	-70.92	-55.78

The series of synthesized compounds labeled 7a to 7j demonstrated satisfactory yields, ranging from 65% to 74%, highlighting the efficiency of the synthetic methodology. The molecular weights of these compounds fell between 321.38 and 411.38 g/mol, which aligns with the presence of various substituents on the parent scaffold, including halogen and functional group modifications. Melting point analysis revealed a range from 174–178 °C (compound 7c) to 230–232 °C (compound 7f), suggesting differences in molecular packing and intermolecular forces. Fluorinated derivatives such as 7f and 7g exhibited relatively higher melting points, likely due to enhanced dipolar interactions. Chromatographic analysis showed Rf values between 0.23 and 0.45; compound 6e, containing a chlorine atom, had the highest Rf value, indicative of lower polarity, whereas compounds like 7g and 7h displayed lower Rf values, reflecting increased polarity. These findings confirm the successful synthesis and reveal how structural variations influence the compounds' physical properties.

The ADME analysis of compounds 7a–7j indicated consistently high gastrointestinal (GI) absorption across the series, supporting their suitability for oral administration. Among them, only compound 6j exhibited the ability to cross the blood-brain barrier (BBB), pointing to potential central nervous system (CNS) activity, while the rest are likely restricted to peripheral action. P-glycoprotein (P-gp) substrate prediction revealed that compounds 7c, 7i, and 7j may be subject to efflux mechanisms, which could influence their bioavailability. Regarding cytochrome P450 (CYP) enzyme interactions, most compounds were predicted to inhibit CYP1A2, CYP2C9, and CYP2D6, suggesting possible metabolic interactions. In contrast, inhibition of CYP2C19 was limited, observed only in compounds 7a and 7e. Notably, compound 6j demonstrated a unique profile with BBB permeability, P-gp substrate potential, and minimal CYP inhibition, highlighting it as a promising candidate for further exploration in CNS-related drug development.

The docking study using AutoDock revealed that the synthesized compounds (7a–7j) showed a range of binding affinities toward the target protein, with values between –6.3 and –8.7 kcal/mol. Notably, compound 7c demonstrated the highest binding affinity at –8.7 kcal/mol, outperforming the standard reference drug Entrectinib (–8.4 kcal/mol), suggesting strong interaction and potential as a lead molecule. Compounds 7i (–8.5 kcal/mol) and 7e (–8.2 kcal/mol) also exhibited comparable or slightly better binding than Entrectinib, indicating favorable binding characteristics. Moderate affinities were observed with compounds 7f (–7.8 kcal/mol), 7b (–7.5 kcal/mol), and 6d (–7.3 kcal/mol). On the other hand, compounds 7a (–6.3 kcal/mol), 7j (–6.5 kcal/mol), 7g and 7h (both –6.8 kcal/mol) displayed lower binding affinities, suggesting weaker interactions with the target. These results highlight the influence of structural differences on binding efficiency and suggest that some of these derivatives may serve as promising candidates for further optimization.

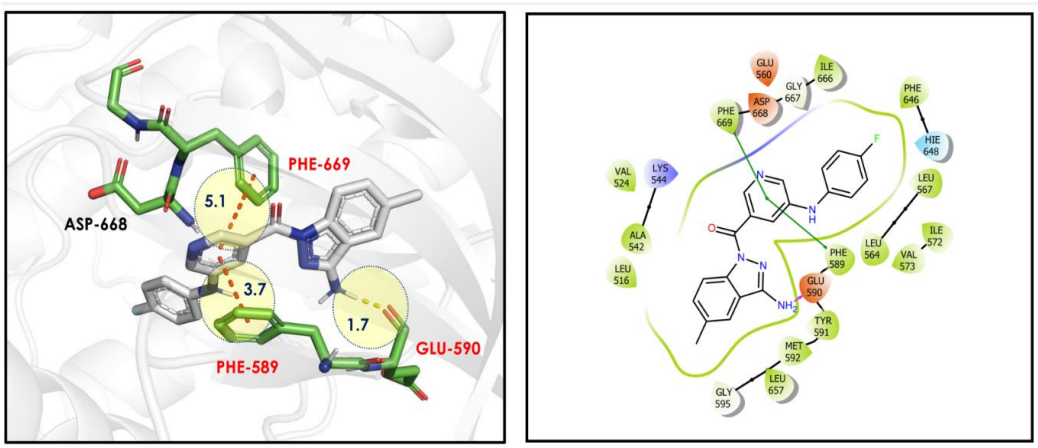

Fig 4. Describes the binding orientation of compound 7g with Crystal structure of Trk A The interaction of PHE 589 (light green), GLU 590 (red), PHE 646 (light green), HIS 648 (light blue) of receptor (PDB Id: 5JFX). Hydrogen bonds are indicated by green dashed lines to key amino acids and π – π interaction is indicated by pink dashed lines.

Chemistry and spectral characterization

A series of (3-amino-5-methyl-1H-indazol-1-yl)(5-substituted-pyridin-3-yl)methanone derivatives (7a–7f) were synthesized and characterized using various spectroscopic techniques including IR, proton H-NMR, 13C-NMR, and mass spectrometry. These compounds were obtained in good yields ranging from 76% to 82% and were isolated as white to off-white crystalline solids with melting points between 174–232 °C, indicating good purity and solid-state stability. The IR spectra of all compounds exhibited characteristic absorption bands for N–H stretching between 3328–3478 cm^{-1}, confirming the presence of amine and indazole N–H groups. Strong carbonyl (C=O) stretches were observed between 1655–1674 cm^{-1}, indicative of the amide linkage in all derivatives. Additional peaks for aromatic C=C and C=N stretching vibrations were consistently seen around 1500–1556 cm^{-1} .The proton H-NMR spectra revealed complex aromatic multiplets in the range of δ 6.0–9.0 ppm, corresponding to various aryl protons, and singlets for methyl (CH_3) groups near δ 2.4–2.5 ppm. Notably, compound 7c, bearing a cyclopentyl substituent, exhibited aliphatic multiplets between δ 1.4–3.8 ppm, confirming the presence of saturated cyclic moieties. Singlets near δ 6.5 ppm corresponded to $–NH_2$ protons, while distinct methyl singlets at ~2.2–2.4 ppm were observed for methyl-substituted phenyl rings (e.g., in 7b and 7d). The 13C-NMR spectra supported the proposed structures, showing resonances for carbonyl carbons near δ 164–165 ppm, aromatic carbons over δ 115–154 ppm, and methyl carbons around δ 20–21 ppm. Compound 7c displayed additional aliphatic carbon signals between δ 23–53 ppm due to the cyclopentyl ring. Mass spectrometric analysis confirmed the molecular weights with M+1 peaks at m/z values consistent with each derivative: 344.40 (7a), 358.40 (7b and 7d), 336.40 (7c), 378.35 (7e), and expected higher values for fluorinated analogues such as 7f. These results collectively support the successful synthesis and structural integrity of the targeted indazole-pyridine hybrid molecules.

Overall, spectral data are in good agreement with the proposed molecular structures, indicating successful formation of the designed compounds. The variation in melting points and spectral shifts further reflects the influence of different aromatic and aliphatic substituents on the electronic and steric environment of the molecules. These derivatives, due to their structural framework incorporating indazole and substituted pyridine moieties, are potential candidates for further pharmacological screening.

Biological activities:

The antiproliferative activity of the synthesized compounds (7a–7j) was assessed against the MCF-7 human breast cancer cell line at various concentrations (10, 20, 40, and 80 µg/mL), using Adriamycin (ADR) as a positive control. The percentage of control cell growth, averaged over three experimental repeats, served as an indicator of each compound's cytotoxic potential.

Among all the tested derivatives, compounds 7b and 7c emerged as the most effective, exhibiting notably negative growth percentages at higher doses. At 40 µg/mL, compound 7b reduced cell growth to –23.22%, and 7c to –28.22%; the inhibition became more pronounced at 80 µg/mL, dropping further to 6.38% and –64.06%, respectively. These results indicate that both compounds possess strong cytostatic or cytotoxic effects on MCF-7 cells, approaching the efficacy seen with the standard ADR, which maintained inhibition levels between –70.92% and –55.78%. Conversely, compound 7a exhibited minimal impact on cell viability, with all values remaining above 90%, pointing to its weak activity or possible biocompatibility. Similarly, 7e and 7f showed limited inhibitory effects, with control growth percentages exceeding 50% even at higher concentrations, suggesting low cytotoxic strength.

Compounds 7d, 7g, 7h, 7i, and 7j showed moderate efficacy, with inhibition generally increasing in a dose-dependent manner. For example, 7d reduced cell growth from 67.70% at 10 µg/mL to 43.52% at 80 µg/mL, indicating moderate cytotoxic potential. Compound 6h, although less active at lower concentrations, showed substantial inhibition at 80 µg/mL (12.26%), reflecting enhanced potency at higher doses.

The control drug, Adriamycin, consistently demonstrated strong anticancer activity across all doses, validating the sensitivity and reliability of the assay system. A slight decrease in inhibitory effect at the highest dose could be attributed to adaptive resistance or saturation of cytostatic impact.

In summary, compounds 7b and 7c displayed promising anticancer properties, potentially due to favourable structural features enhancing their interaction with cellular targets. The negative growth percentages indicate not only growth arrest but also the likelihood of induced cytotoxicity. Future work should explore mechanistic pathways such as apoptosis induction, cell cycle disruption, and molecular docking studies to better understand their mode of action. Even compounds with moderate effects may serve as useful scaffolds for further optimization or could be investigated in combination therapies. Growth inhibition curve of MCF-7 human breast cancer cells treated with synthesized compounds (7a–7j), Doxorubicin, and ADR given in Figure 5 and the image shows MCF-7 breast cancer cells following treatment with the synthesized compound 7c, 7i given in Figure 6.

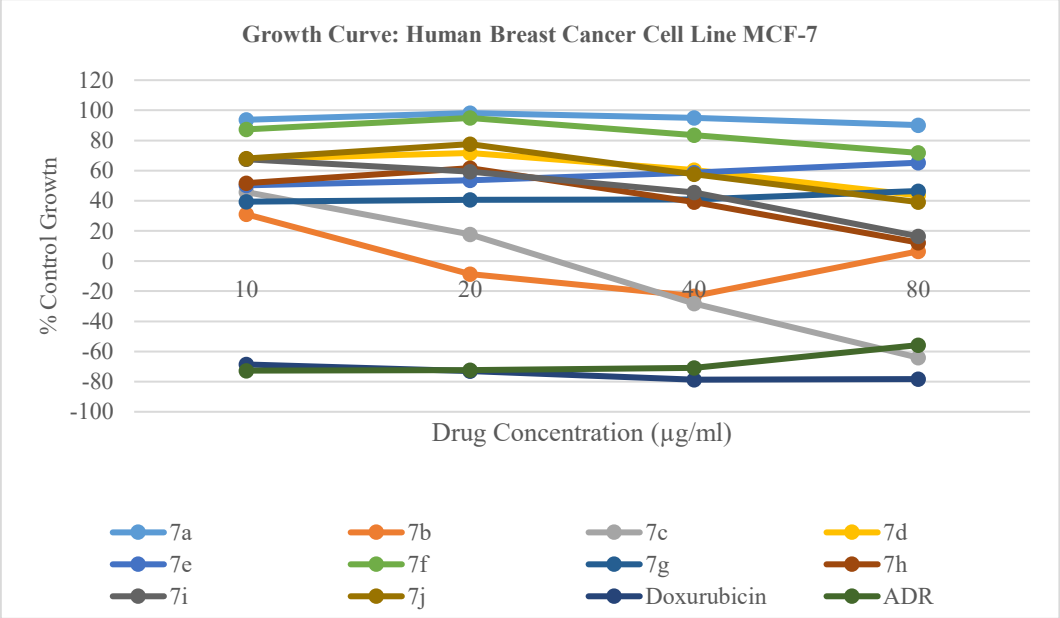

Fig 5. Growth inhibition curve of MCF-7 human breast cancer cells treated with synthesized compounds (7a–7j), Doxorubicin, and ADR. This figure illustrates the dose-dependent effects of various synthesized compounds (7a–7j) on the proliferation of MCF-7 breast cancer cells. The growth inhibition was measured at four different concentrations: 10, 20, 40, and 80 µg/mL, and expressed as % control growth.

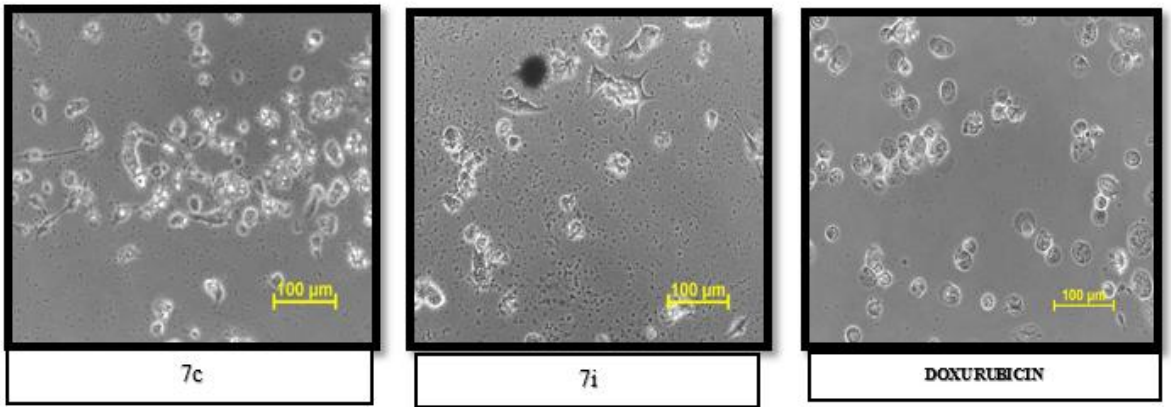

Fig 6. ***Microscopic evaluation of MCF-7 cells.*** The image shows MCF-7 breast cancer cells following treatment with the synthesized compound 7c, 7i. Morphological alterations such as cell shrinkage, rounding, and detachment from the surface are evident, indicating potential cytotoxic effects. A notable reduction in cell confluency suggests that compound 7c and 7i induces cell death or inhibits proliferation. The scale bar represents 100 µm, providing a reference for cellular size and spatial distribution. Microscopic image of cancer cells treated with Doxorubicin

(Dox). The figure displays a phase-contrast microscopic image of cells post-treatment with Doxorubicin, a standard chemotherapeutic agent, to serve as a reference control.

Structure-activity relationship (SAR):

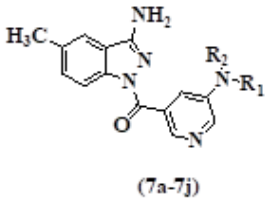

(7a-7j)

Comp.	Amines
7a	Aniline
7b	p-Toluidine
7c	Cyclopentylamine
7d	o-Toluidine
7e	2-Chloroaniline
7f	4-(Trifluoromethyl)aniline
7g	4-Fluoroaniline
7h	4-Methoxyaniline
7i	Morpholine
7j	Pyrrolidine

Among the synthesized derivatives, compounds **7c** and **7b** exhibited notable cytotoxic effects, with a pronounced decline in MCF-7 cell viability observed as the concentration increased. The binding affinities for 7c and 7b were calculated as –8.7 kcal/mol and –7.5 kcal/mol, respectively, indicating favorable interactions with the target. **Compound 7c** demonstrated the highest antiproliferative activity, reducing cell growth to below 0% at 40 and 80 µg/mL. Structurally, **7c** features an aliphatic cyclopentane ring directly linked to a pyridine moiety, which may contribute to its enhanced activity. **Compound 7b** contains a methyl group at the para position of the benzene ring, an electron-donating substituent likely responsible for its significant in vitro cytotoxicity and growth inhibition. Additionally, the presence of an electron-withdrawing fluorine atom at the para position in **compound 7g** also appears to enhance anticancer activity. In contrast, derivatives like **7a** (unsubstituted phenyl ring) and **7d** (fluorine substitution at the ortho position) displayed weaker cytotoxic effects, with cell viability remaining above 60–80%, suggesting reduced anticancer potential.

Conclusion

The present study successfully synthesized a novel series of compounds **(7a–7j)** with good yields and well-characterized physicochemical properties. Variations in melting points, Rf values, and molecular weights reflected the influence of different substituents, particularly halogens and functional groups, on molecular interactions and structural stability. Fluorinated derivatives, for instance, exhibited higher melting points due to enhanced dipole interactions, while chromatographic behaviour corresponded with the polarity of the substituents.

Molecular docking studies provided valuable insights into the interaction of these compounds with a cancer-related target protein. Compound **7c** demonstrated the highest binding affinity (–8.7 kcal/mol), surpassing the standard drug Entrectinib, while compounds **7i** and **7e** also showed comparable binding profiles. These results highlight the significance of specific substituents, such as cyclopentane and halogen groups, in enhancing binding interactions and suggest promising lead structures for further development.

ADME predictions confirmed favorable pharmacokinetic properties for most compounds, with high gastrointestinal absorption and minimal CYP inhibition, ensuring good oral bioavailability and reduced metabolic liability. Compound **7j** stood out for its blood-brain barrier permeability and minimal CYP interactions, indicating its potential for central nervous system applications.

Biological evaluation against MCF-7 breast cancer cells revealed that compounds 7b and 7c exhibited strong cytotoxic effects, with dose-dependent inhibition comparable to the standard Adriamycin. Moderate activity was observed in compounds 7d, 7g, 7h, and 7i, while 7a, 7e, and 7f showed limited impact. These findings suggest that structural modifications significantly influence antiproliferative efficacy.

In conclusion, compounds **7b** and **7c** emerged as the most promising candidates, warranting further investigation into their mechanisms of action, including apoptosis and cell cycle effects. The moderate-to-strong cytotoxicity observed among several derivatives also provides a foundation for further optimization and structure-activity relationship (SAR) studies.

Acknowledgment

The first author is thankful to Parul University, Vadodara, and Gujarat for providing intramural grant and providing infrastructure facility for the research work.

Funding

The research leading to these results received funding from the Parul University, Vadodara, Gujarat, India under Grant No. CR4D/IMSL/0003.

Ethical Approval

Not Applicable

Informed consent
Not Applicable

Supplementary Information
Additional material related to this article can be found, in the online version.

Human and Animal Right
No animal/humans were used for studies that are the basis of this research

Conflict of Interest
On behalf of all authors, the corresponding author states that there is no conflict of interest.

References

1. Rebecca L. Siegel, Angela N. Giaquinto, Ahmedin Jemal (2024) Cancer statistics, 2024. CA: A Cancer Journal for Clinicians. 74: 12–49. https://doi.org/10.3322/caac.21820
2. Angela N. Giaquinto, Hyuna Sung, Lisa A. Newman, Rachel A. Freedman, Robert A. Smith, Jessica Star, Ahmedin Jemal, Rebecca L. Siegel (2024) Breast cancer statistics. CA: A Cancer Journal for Clinicians. 74: 465–519. https://doi.org/10.3322/caac.21834
3. Kulothungan V, Ramamoorthy T, Sathishkumar K, Mohan R, Tomy N, Miller GJ, Mathur P (2024) Burden of female breast cancer in India: estimates of YLDs, YLLs, and DALYs at national and subnational levels based on the national cancer registry programme. Breast Cancer Research and Treatment. 205: 323–332. https://doi.org/10.1007/s10549-024-07264-3
4. Sarkar S, Horn G, Moulton K, Oza A, Byler S, Kokolus S, Longacre M (2013) Cancer development, progression, and therapy: An epigenetic overview. International Journal of Molecular Sciences. 14: 21087–21113. https://doi.org/10.3390/ijms141021087
5. Sharma V, Sharma PC, Kumar V (2016) In silico molecular docking analysis of natural pyridoacridines as anticancer agents. Advances in Chemistry. 2016: 1–9. https://doi.org/10.1155/2016/5409387
6. Puri S, Sawant S, Juvale K (2023) A comprehensive review on the indazole based derivatives as targeted anticancer agents. Journal of Molecular Structure. 1284: 112–138. https://doi.org/10.1016/j.molstruc.2023.135327
7. Al-Tuwaijri HM, Al-Abdullah ES, El-Rashedy AA, Ansari SA, Almomen A, Alshibl HM, Haiba ME, Alkahtani HM (2023) New indazol-pyrimidine-based derivatives as selective anticancer agents: Design, synthesis, and in silico studies. Molecules. 28: 3664–3683. https://doi.org/10.3390/molecules28093664
8. Pandiyan S, Wang L (2024) In-silico design of novel potential HDAC inhibitors from indazole derivatives targeting breast cancer through QSAR, molecular docking and pharmacokinetics studies. Computational Biology and Chemistry. 110: 123–135. https://doi.org/10.1016/j.compbiolchem.2024.108035
9. Panchal I, Tripathi RKP, Yadav MR, Valera M, Parmar K (2024) Design, synthesis, and biological and in silico evaluation of novel indazole-pyridine hybrids for the treatment of breast cancer. Current Computer-Aided Drug Design. 21: 211–225. https://doi.org/10.2174/0115734099308839240724100224
10. Wei W, Liu Z, Wu X, Gan C, Su X, Liu H, Que H, Zhang Q, Xue Q, Yue L, Yu L, Ye T (2021) Synthesis and biological evaluation of indazole derivatives as anti-cancer agents. RSC Advances. 11: 15675–15687. https://doi.org/10.1039/D1RA01147B
11. Saghdani N, El Brahmi N, El Abbouchi A, Haloui R, Elkhattabi S, Guillaumet G, El Kazzouli S (2024) Design, synthesis, and evaluation of EA-sulfonamides and indazole-sulfonamides as promising anticancer agents: Molecular docking, ADME prediction, and molecular dynamics simulations. Chemistry. 6: 1396–1414. https://doi.org/10.3390/chemistry6060083
12. La MT, Hoang VH, Sahu R, Nguyen CT, Nam G, Park HJ, Park M, Kim YJ, Kim JY, Ann J, Seo JH, Lee J (2024) Discovery of indazole inhibitors for heat shock protein 90 as anti-cancer agents. European Journal of Medicinal Chemistry. 276: 117194–117214. https://doi.org/10.1016/j.ejmech.2024.116620
13. Mehta K, Hegde M, Girisa S, Ishwa R, Alqahtani MS, Abbas M, Shakibaei M, Sethi G, Kunnumakkara AB (2024) Targeting RTKs/nRTKs as promising therapeutic strategies for the treatment of triple-negative breast cancer: Evidence from clinical trials. Military Medical Research. 11: 76–101. https://doi.org/10.1186/s40779-024-00582-z
14. Maund SL, Sokol ES, Houle AA, Ross JS, Wilson TR (2022) NTRK gene fusions are detected in both secretory and non-secretory breast cancers. Pathology International. 72(3): 187–192. https://doi.org/10.1111/pin.13204
15. Kyker-Snowman K, Hughes RM, Yankaskas CL, Cravero K, Karthikeyan S, Button B, Waters I, Rosen DM, Dennison L, Hunter N, Donaldson J, Christenson ES, Konstantopoulos K, Hurley PJ, Croessmann S, Park BH (2020) TrkA overexpression in non-tumorigenic human breast cell lines confers oncogenic

and metastatic properties. Breast Cancer Research and Treatment. 179: 631–642. https://doi.org/10.1007/s10549-019-05506-3

16. Skehan P, Storeng R, Scudiero D, Monks A, McMahon J, Vistica D, Warren JT, Bokesch H, Kenney S, Boyd MR (1990) New colorimetric cytotoxicity assay for anticancer-drug screening. Journal of the National Cancer Institute. 82: 1107–1112. https://doi.org/10.1093/jnci/82.13.1107

Supplementary Files

This is a list of supplementary files associated with this preprint. Click to download.

- supplementarymaterial.docx